AGU PUBLICATIONS

Geophysical Research Letters

RESEARCH LETTER
10.1002/2017GL074384

Key Points:
- Detailed observations are presented of extraordinary rich turbulent overturning near a Mid-Atlantic Ridge hydrothermal vent system
- Preconditioning characteristics are originating from 400 m above the bottom before the arrival of an upslope moving frontal bore
- The more intense turbulence higher up in the water column is suggested to lead to strong dispersion of the natural hydrothermal plume

Correspondence to:
H. van Haren,
hans.van.haren@nioz.nl

Citation:
van Haren, H., G. Duineveld, and H. de Stigter (2017), Prefrontal bore mixing, *Geophys. Res. Lett.*, *44*, 9408–9415, doi:10.1002/2017GL074384.

Received 31 MAY 2017
Accepted 23 AUG 2017
Accepted article online 29 AUG 2017
Published online 18 SEP 2017

Prefrontal bore mixing

Hans van Haren[1], Gerard Duineveld[1], and Henko de Stigter[1]

[1]Royal Netherlands Institute for Sea Research (NIOZ) and Utrecht University, Den Burg, Netherlands

Abstract Rainbow Ridge, a 1950 m deep upthrusted ultramafic block along the axis of the Mid-Atlantic Ridge, has an active hydrothermal vent system at 2400 m on its western slope. However, within 1 km from the vent excessive temperatures are barely measurable, probably due to strong turbulent mixing. This mixing is studied here using a 400 m long high-resolution temperature sensor array moored with a 600 m ranging 75 kHz acoustic Doppler current profiler. Rich internal wave turbulence was recorded, characterized by 100–200 m upshoots and >200 m large overturning in particular near the end of the warming phase of the up and down moving tide. These highly nonlinear internal waves of tides interacting with buoyancy frequency waves extend up to 400 m above the sloping bottom of the ridge. While a turbulent "bottom boundary layer" could barely be defined, the more intense turbulence higher up in the water column is suggested to lead to the strong dispersion of the hydrothermal plume.

1. Introduction

Hydrothermal vents occurring along the edges of tectonic plates are important sources of metal-rich minerals in the water column and sediment of the oceans [*Sander and Koschinsky*, 2011, 2016]. Depending on the geological settings of the vent controlling strength, temperature, and geochemistry of the outflow, areas around vents may become enriched in minerals, specifically seafloor massive sulfide (SMS) deposits, which precipitate from the exhalant flow. Concern about the impact of future mining of SMS deposits plus the lack of data on the background community and environment has triggered a series of papers reviewing potential risks [e.g., *Boschen et al.*, 2013; *Collins et al.*, 2013] in combination with new studies including the Dutch Towards Responsible ExtrAction of Submarine Resources (TREASURE) project which the present study is part of. Since as yet there are no real deep-sea mining plumes to be studied, we focused on the dispersion of the natural hydrothermal plume ejected by the Rainbow hydrothermal vent, located on the Mid-Atlantic Ridge (MAR) about 500 km SW of the Azores. In particular, we focused on deep-sea turbulent mixing mechanisms.

Earlier studies showed that natural hydrothermal temperature signals are rapidly lost away from very active fields exerting near-boiling point waters, like Rainbow vent [*German et al.*, 1996; *Khripounoff et al.*, 2001]. Not more than 1000 m downstream away from the Rainbow vent system with estimated ~1 GW heat flux, no indication could be traced in moored temperature sensors. This contrasts with other tracers, as Rainbow vent waters have unusually high contents of Fe, Mn, Cl, and CH_4 that are detectable over much longer distances [*Desbruyères et al.*, 2000]. Turbidity or nephelometer sensors register suspended particles tens of kilometers away from the vents [*German et al.*, 1996; *Thurnherr and Richards*, 2001]. The particles are observed in a layer of about 200 m thick, later reorganized in thinner layers between 2000 and 2200 m, after being emitted from the 2400 m deep vent system. They flow northward following the bottom contours of the 1950 m high Rainbow Ridge (RR), until they disperse into the deep axial basin NE of the ridge.

This difference in traceability between parameters may have to do with the rapid masking of the density/temperature field by large-scale flows and, more likely, by internal wave activity supported by the density stratification. Large internal waves are reported in the area [*Thurnherr and Richards*, 2001]. Near bottom topography in general, internal waves are expected to break and generate irreversible turbulent mixing [*Eriksen*, 1982; *Thorpe*, 1987; *Aucan et al.*, 2006; *van Haren and Gostiaux*, 2012; *Dale and Inall*, 2015]. Above bottom slopes steeper than those of internal tides, high-resolution (1 Hz sampled, 1 m vertical distance, and <0.1 mK noise level) temperature observations fit a shear turbulence inertial subrange [*Cimatoribus and van Haren*, 2015]. A break in turbulence scaling is observed at the buoyancy scale $U/N \sim 100$ m, U and N typical large-scale current speed and buoyancy frequency, respectively. Over larger ranges, scale-independent internal waves dominate. Over smaller ranges, toward the about tenfold smaller Ozmidov scale, turbulent motions dominate. This suggests a "boundary layer scale" of at least 100 m. This scale has been confirmed

in recent numerical modeling of internal wave breaking at a supercritically steep slope, in which turbulence extended to about 250 m above the bottom [*Winters*, 2015].

In the present paper, we study the characteristics of such a "boundary layer" using high-resolution temperature *T* sensors over 400 m moored with an acoustic Doppler current profiler (ADCP) ranging over 600 m. We are especially interested in the particulars of internal wave-induced turbulence near the Rainbow hydrothermal vent and possible consequences for plume behavior. Since the vent is located on the slope of a ridge, the focus is on the transition between off-ridge "warming phase" and on-ridge "cooling phase" motions to detail some of the largest turbulence found during a tidal period.

2. Materials and Methods

Observations were made using a single mooring deployed from 28 June to 10 July 2016 at 36°14.86′N, 33°52.61′W, 2240 m water depth, on the northwestern slope of RR. The mooring site was about 3 km NE and downstream from the Rainbow hydrothermal vents, with the anchor weight positioned about 150 m shallower than the vents and 300 m below the top of the ridge, which is 3 km due south (Figure 1). The local bottom slope is $\beta \approx 0.22 = 13°$.

The mooring consisted of a 710 m nylon-coated steel cable extended vertically between a single heavy top buoy and a 550 kg anchor weight. The net buoyancy of the mooring was 250 kg, and the net anchor was 200 kg. In the lower 398 m of the mooring cable 200 "NIOZ4" self-contained high-resolution *T* sensors were taped every 2 m. The lowest sensor was at 8 m above the bottom. The sensors sampled at a rate of 1 Hz, with a precision better than 5×10^{-4}°C and a noise level of $<1 \times 10^{-4}$°C (see *van Haren et al*. [2009] for the predecessor "NIOZ3" with similar characteristics).

Every 4 h all *T* sensors were synchronized to a standard clock, so that their times were <0.02 s off and the 398 m nearly true vertical profile was measured every second. Seventeen sensors showed calibration or electronic problems, and their data were linearly interpolated. After correction for slight compressibility and drift effects of <1 mK/mo, the *T* data were converted into "conservative" (~potential) temperature data Θ [*Intergovernmental Oceanographic Commission (IOC), Scientific Committee on Oceanic Research (SCOR), and International Association for the Physical Sciences of the Oceans (IAPSO)*, 2010]. They were used as a tracer for density anomaly σ_2 variations referenced to 2000 dbar following the relation $\delta\sigma_2 = \alpha\delta\Theta$, where $\alpha = -0.075 \pm 0.001$ kg m^{-3}°C^{-1} denotes the apparent thermal expansion coefficient under local conditions. This tight linear relation was established from shipborne conductivity-temperature-depth (CTD) profile near the mooring site at about 3 km from Rainbow vent. Implicitly, these data thus confirmed historic observations [*German et al*., 1996; *Khripounoff et al*., 2001] that the vent is not traceable in temperature at distances >1 km away from it horizontally. In the data sets under investigation, salinity intrusions disturbing this relationship did not occur.

The number of *T* sensors and their spacing of 2 m, in combination with their low noise level, allowed for the quantification of turbulence by estimating turbulence dissipation rate ε and vertical eddy diffusivity K_z via the reordering of unstable overturns making every 1 Hz sampled "density"-(temperature) profile a statically stable one [*Thorpe*, 1977]. For details of the method for moored thermistor sensor data using the standard oceanographic parameterizations, see *van Haren and Gostiaux* [2012]. It involved an Ozmidov/Thorpe overturning scale ratio of 0.8 and a mixing efficiency of 0.2. These values were established from ocean observations after sufficient averaging [*Dillon*, 1982; *Oakey*, 1982; *Mater et al*., 2015]. This is understandable as the ocean is a high Reynolds number environment having values between 0.1 and 10 million that are much higher than achievable in numerical modeling. Ocean turbulence is also a mix of free convective and especially shear-induced motions [*Cimatoribus and van Haren*, 2015], in particular above sloping topography where rapid restratification following internal wave breaking ensures high mixing efficiencies [*van Haren et al*., 1994; *Slinn and Riley*, 1996; *Cyr and van Haren*, 2016]. In the following, averaging over time is denoted by […], averaging over depth range by <…>.

In addition to the *T* sensors, the mooring was equipped with a downward "looking" 75 kHz Teledyne/RDI ADCP in the top buoy of the mooring and a single-point Nortek AquaDopp current meter at 6 m above the bottom. The ADCP sampled 120 vertical bins of 5 m each at a rate of once per 60 s. The 20° slanted beams of the ADCP caused an averaging over several hundreds of meters horizontally, so that its current measurements only resolved the large spatial scales. The single-point current meter also sampled the 3-D velocity components [*u*, *v*, *w*] but from a volume of about 0.5 m^3 at a rate of once per 10 s.

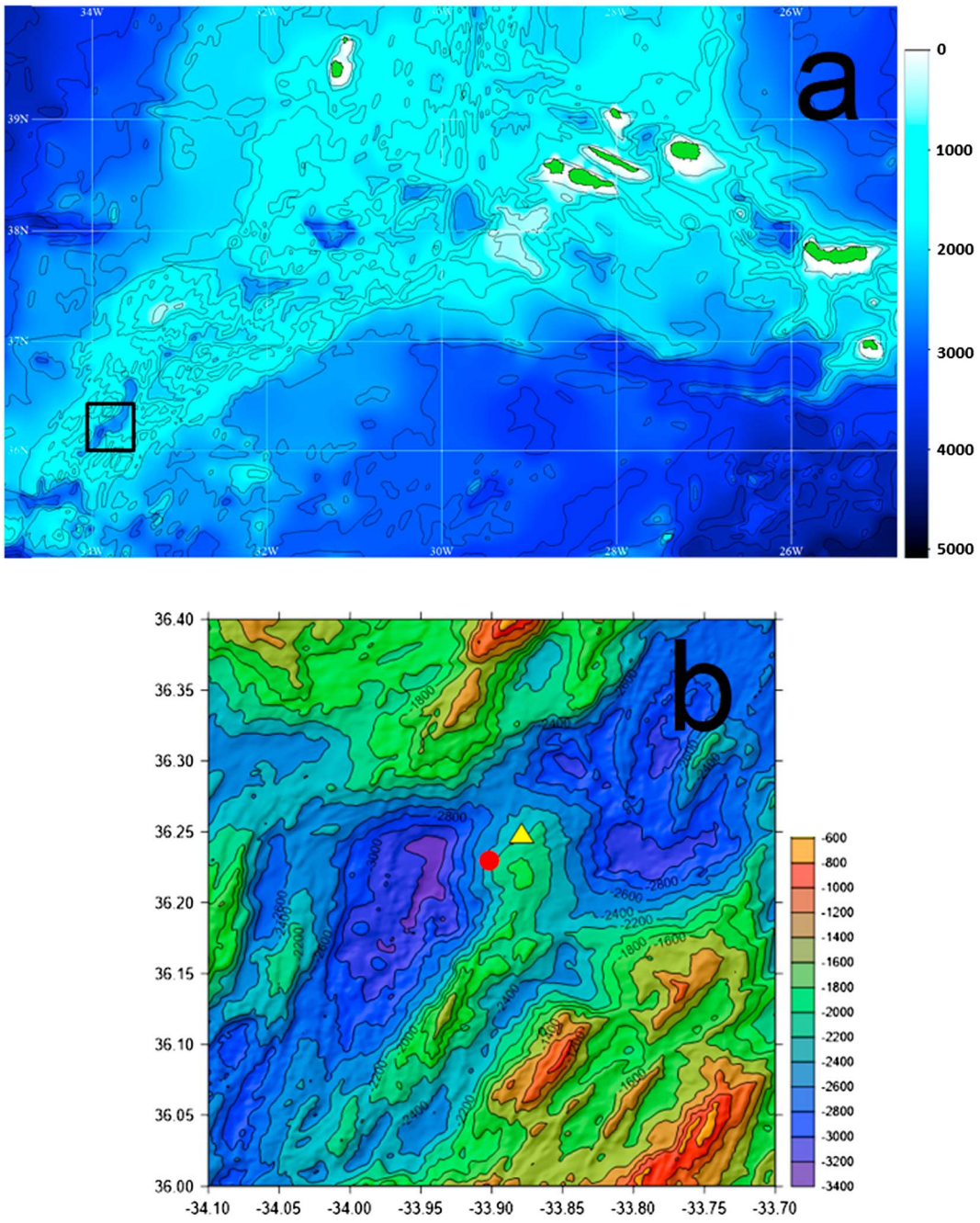

Figure 1. Bathymetric map of the Rainbow Ridge in the Azores area, part of the Mid-Atlantic Ridge, North Atlantic Ocean, with the location of the mooring indicated by the yellow triangle on its north slope and the hydrothermal vent by the red dot. (a) GEBCO (v. 8) data. (b) Multibeam data, 100 × 100 m grid.

3. Observations

Water motions around the RR are dominated by the semidiurnal tide and its fourth-diurnal harmonic. Inertial motions are less energetic. Horizontal near-bottom current amplitudes reach 0.3 m s^{-1} (Figure 2a), vertical currents peak at ±0.1 m s^{-1} (Figure 2b), while isotherm displacements reach 200 m from crest to trough (Figure 2c). Near the bottom, the tidal current "ellipse" has a cross-slope amplitude of 0.15 m s^{-1} and an along-slope amplitude of 0.10 m s^{-1}, while being near circular with amplitude of 0.10 m s^{-1} at distances of 150 m and more from the bottom. Thus, around the 1950 m deep ridge internal tides are not small and their pattern appears very regular. The regularity of the motions is also reflected in the vertically averaged

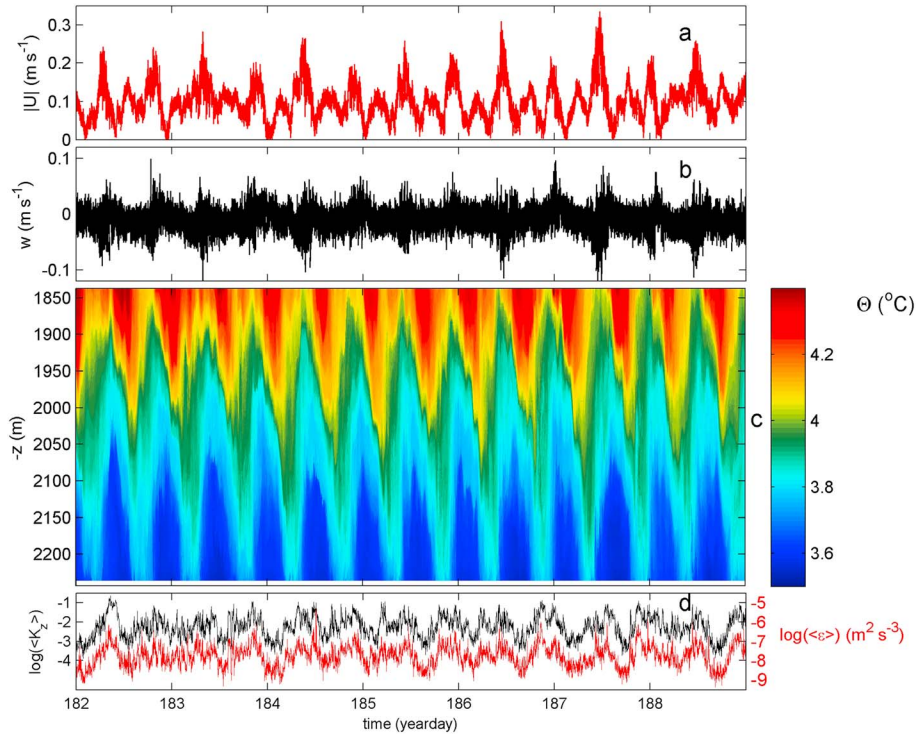

Figure 2. Seven day data overview. (a) Current amplitude measured at the near-bottom current meter. (b) Vertical current (positive up). (c) Conservative temperature from measurements by the *T* sensor array. (d) Logarithms of vertically averaged turbulence dissipation rate (red, scale to the right) and eddy diffusivity (black), from the data in Figure 2c.

turbulence parameters, which generally shows high values around the transition from the downward, warming phase of the tide to the upward, cooling phase (Figure 2d). As will be demonstrated below in two detailed examples, 1 day apart of the transition from the warming to cooling tidal phases, a clear change is observed around 1900 m. Shallower, above the ridge crest, internal wave motions are more or less regular. Deeper, motions occur in short bursts which are related to the highly nonlinear internal waves that dominate the lower 300 m above the bottom, at the mooring site. Turbulence peaks such as occurring around the upslope propagating nonlinear frontal bore and its trailing cooler waters as on day 182.3 have been well documented [e.g., *van Haren and Gostiaux*, 2012]. Here we focus on the prefrontal turbulent mixing as it is found more pronounced than in other observations above sloping topography.

Above the slope of RR the last 2 h of the warming phase typically show a very smooth high-frequency internal wave, here illustrated for around day 186.8, growing in amplitude with relatively little shear-induced turbulence in the near-homogeneous layers between the thin strongly stratified filaments (Figure 3). The vertical size of the thin filaments is $<$10 m, which is similar to layering in turbidity data. However, such layering is only found in limited CTD stations close to Rainbow vent and not near the mooring site (not shown), in contrast with observations by *German et al*. [1996]. At some point the high-N stratification interfaces slant with respect to the isotherms (Figure 3b), but it is difficult to establish whether they are the result of collapsing mixing patches or internal wave straining (or a combination of both). The warmer water coming from above is considerably more turbulent. However, most turbulent overturning is generated after the collapse of the high-frequency wave, in this example generating a 200 m high overturn that just not touches the bottom as stratification is visible near the lower *T* sensors (Figure 3b). The following nonlinear near-bottom cold-water front, also about 200 m high eventually, does not arrive until an hour later. It shows somewhat less intense turbulence.

One day later, exemplifying the variability between the tidal periods, the smooth high-frequency internal wave near the end of the warming phase shoots up 150 m and breaks with turbulent fingers on day 187.87 (Figure 4). A large 200 m overturn as in the previous example is not visible, but the waters trailing the single high-frequency internal wave are turbulent over that range around 2050 m for 1.5 h between days 187.85

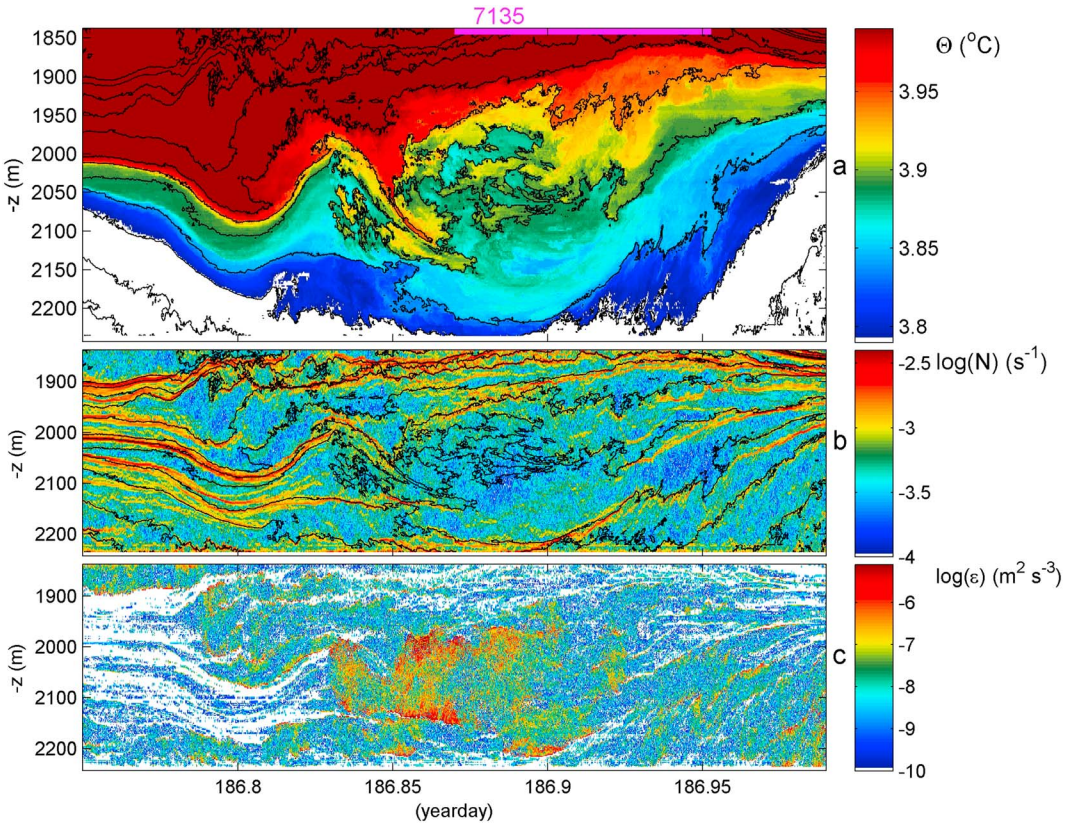

Figure 3. Quarter-day detailed example of transition from off-ridge to on-ridge flow. (a) Conservative temperature. Contours are drawn every 0.05°C. The purple bar denotes the mean buoyancy period, in seconds. (b) Logarithm of buoyancy frequency from reordered Θ profiles with contours from Figure 3a repeated. (c) Logarithm of turbulence dissipation rate.

and 187.91, again not touching the bottom. The bottom-touching cool-water upslope propagating front arrives on day 187.97 and extends some 250 m up.

The downward moving relatively strong turbulence is also reflected in vertical motions, demonstrating its effects above the top of RR (Figure 5). The larger panels in Figure 5, each depicting 1 day, show a break in high-frequency and tidal internal wave behavior at 1850 ± 50 m. The nonlinearity of the internal tides is well visible in the lower 400 m as the temperature contours appear almost as sawtooths. The internal tide is modulated with the clearly visible internal waves near the mean buoyancy frequency that appear as vertical stripes in *w* thus having a large vertical wavelength with little apparent phase delay, especially in the upper half of the figure. There the buoyancy period is about 5000 s, while 17 *w* crests are counted in each panel. In this depth range, the horizontal current components demonstrate a contrasting slanting of tidal crests (not shown) from which a vertical phase speed of 0.012 m s^{-1} is computed. These components give little vertical phase delay in the lower half (not shown), where the vertical current in Figure 5 shows tidally periodic crests that are slanted at about the same rate as those of the horizontal components above. In the lower layer, the tide dominates in modulating *N* waves in *w*, here over nearly the entire *T* sensor range of 400 m. The warming downgoing phase ends when the tide and the near-*N* wave are maximally strained, with downward motions below 2050 m and upward motions above, followed by upward motions leading to the upshoot of the near-*N*-wave crest before collapsing into turbulent overturning.

The vertical and time mean turbulence values from the two periods in Figure 5 do not vary significantly from each other or from the longer period means (Table 1). Only when shorter periods are considered, like in Figures 3 and 4, turbulence values vary by more than one standard deviation: around the transition from warming to cooling tidal phase 6-hourly averaged turbulence values are 2–3 times the values given in Table 1. Although in the vertical too, variations are within the standard deviations for turbulence

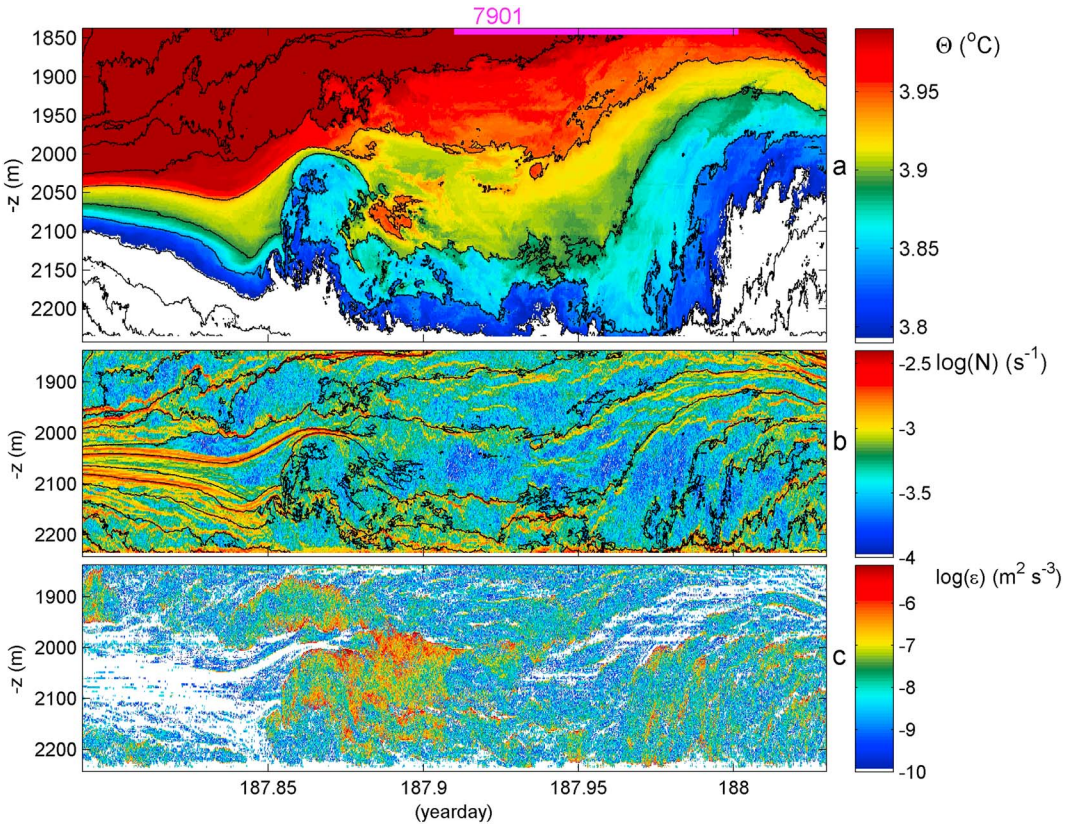

Figure 4. As Figure 3 but exactly two semidiurnal lunar periods later.

dissipation rate, being slightly larger near the bottom and only significantly decreasing above 300 m above the bottom, it is seen that higher diffusivity values by a factor of 2–3 compared to near-bottom values are consistently found around 200–300 m above the bottom. The 100 m mean buoyancy frequency is lowest near the bottom, by a factor of 0.8 times values higher up. In contrast, shortest small-scale buoyancy periods evidencing thin layers are regularly observed in the lower 100 m near the bottom.

4. Discussion

The present observations are somewhat different from previous internal wave breaking observations over steep topography of which the turbulence was dominated by the half-hour passage of a nonlinear near-bottom frontal bore leading the cooling phase of the main carrier wave motion [e.g., *van Haren and Gostiaux*, 2012]. Here generally most diffusivity (but not dissipation rate) is observed 200–300 m away from the bottom, even though being associated with the preconditioning of nonlinear frontal passages: beautiful turbulent mixing is found during the 2–3 h transition from warming to cooling tidal phases. This mixing is observed to occur on a more regular, tidal basis than frontal bore occurrences, even though the precise overturning varies every different tidal period.

The interaction between the near-buoyancy frequency and semidiurnal tidal internal waves is observed to lead to the turbulent upshoot and ~200 m large following overturn that characterize the off-bottom turbulence in the transition from warming to cooling phases. This turbulence is not a result from hydraulic control of the tidal flow over the ridge, as (cf. Table 1) $\beta N \approx 1.5\sigma_{M2}$, <2–$3\sigma_{M2}$ or not enough time for the vertical signal to propagate before the tide reversal [e.g., *Inall et al.*, 2005; *Legg and Klymak*, 2008]. The characteristics of the nonlinear wave development are reminiscent of those over long slopes well below topographic crests [e.g., *van Haren et al.*, 2015; *Winters*, 2015]. Over such long slopes, topography is found to be steeper "supercritical" than the slope of the large-scale carrier wave, here the tide, with large turbulence generation by nonlinear wave breaking. Here the bottom slope of 0.22 is supercritical for internal tides as for given stratification the latter have a slope of approximately 0.16. The lower 300 m daily averaged turbulence values are about a

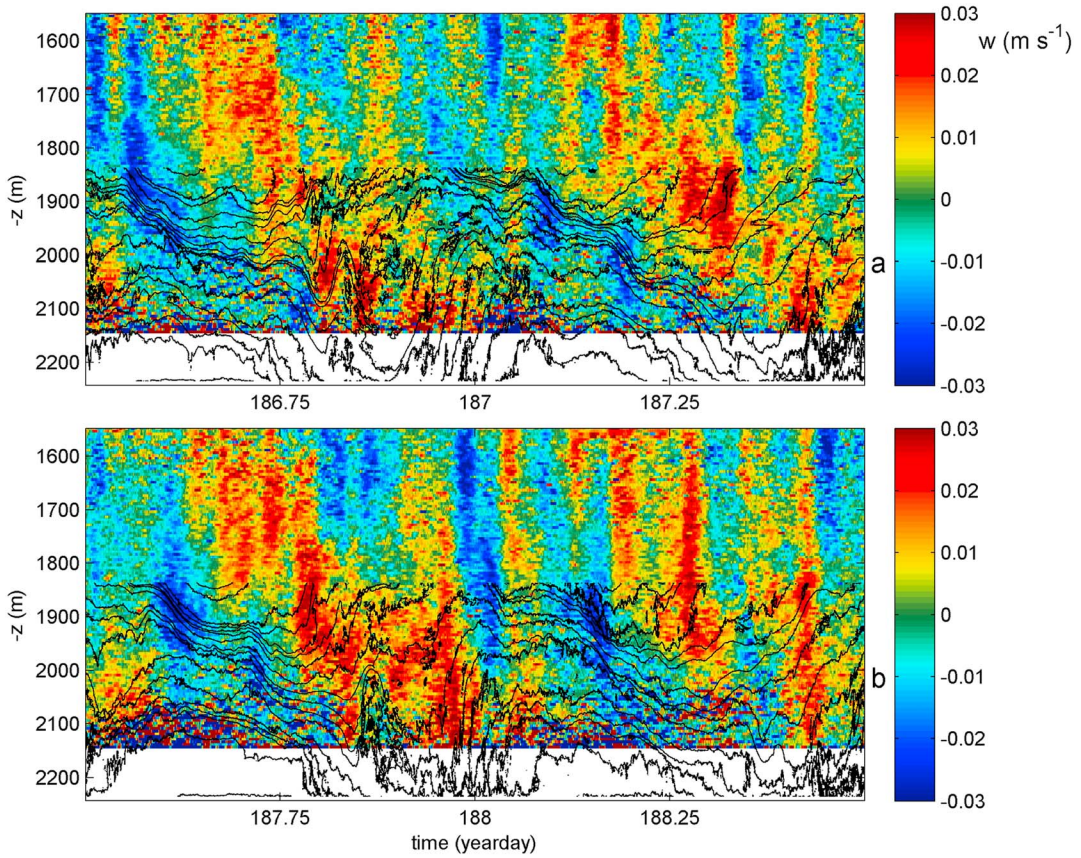

Figure 5. Two different days of vertical current measurements by ADCP, smoothed over 600 s intervals. The black lines are conservative temperature contours every 0.05°C from the *T* sensor data. (a) Day 186.5–187.5, which includes the quarter-day period of Figure 3 in its center. (b) Day 187.5–188.5, which includes the quarter-day period of Figure 4.

quarter of those observed around 2200 m water depth at a supercritical slope of Mount Josephine [*van Haren et al.*, 2015]. Clearest difference is the more regular tidal periodicity of the turbulence found here and its dominance in the interior. As such, it is akin to turbulence observations from atop Hawaiian Ridge, where turbulent overturning was also observed extending several hundreds of meters above the bottom [*Aucan et al.*, 2006; *Klymak et al.*, 2008]. Although their near-bottom eddy diffusivity values from spring tides are comparable with the present data, they decreased with height above the bottom, in contrast with the present data and with MAR data of *Dale and Inall* [2015].

The average amount of turbulent mixing is not particularly small compared to other ocean areas with steep bottom topography, and values are still 100 times larger than found in the open ocean interior [e.g., *Gregg*, 1989]. The interaction between internal tides and high-frequency internal waves near the buoyancy

Table 1. Vertical and Time Mean Turbulence Estimates for 1 (of Figure 5a) and 4 Days and Vertical Ranges of 100 m of Moored *T* Data[a]

Period (yd)	Hght ab (m)	$[<\varepsilon>]$ ($m^2\ s^{-3}$)	$[<K_z>]$ ($m^2\ s^{-1}$)	$[<N>]$ (s^{-1})	Min. Per (s)
186.5–187.5	308–406	$1.7 \pm 1.3 \times 10^{-8}$	$1.2 \pm 0.4 \times 10^{-2}$	$1.2 \pm 0.1 \times 10^{-3}$	1213
	208–306	$5 \pm 3 \times 10^{-8}$	$1.7 \pm 0.6 \times 10^{-2}$	$1.1 \pm 0.1 \times 10^{-3}$	1227
	108–206	$4 \pm 3 \times 10^{-8}$	$1.4 \pm 0.5 \times 10^{-2}$	$9.3 \pm 1 \times 10^{-4}$	1497
	8–106	$6 \pm 4 \times 10^{-8}$	$5 \pm 2 \times 10^{-3}$	$9.0 \pm 1 \times 10^{-4}$	1365
185.5–189.5	308–406	$1.9 \pm 1.5 \times 10^{-8}$	$1.3 \pm 0.5 \times 10^{-2}$	$1.1 \pm 0.1 \times 10^{-3}$	1232
	208–306	$4 \pm 3 \times 10^{-8}$	$1.5 \pm 0.6 \times 10^{-2}$	$1.1 \pm 0.1 \times 10^{-3}$	1227
	108–206	$4 \pm 3 \times 10^{-8}$	$1.3 \pm 0.5 \times 10^{-2}$	$9.6 \pm 1 \times 10^{-4}$	1446
	8–106	$5 \pm 3 \times 10^{-8}$	$5 \pm 2 \times 10^{-3}$	$9 \pm 1 \times 10^{-4}$	910

[a]yd = yearday, hght ab = height above the bottom, Min. Per = minimum short-scale, 2 m scale buoyancy period.

frequency affects turbulence up to about 400 m from the topography as found in observations [*Klymak et al*., 2008; *van Haren*, 2017; this study] and in numerical modeling [*Winters*, 2015]. In this context, it is difficult to speak of a turbulent "bottom boundary layer," the turbulence commencing so far above the bottom, being highly variable in time and with considerable mixing not directly touching the bottom. Here buoyant plumes dispersion seems most affected by prefrontal bore turbulent mixing at 100 to 300 m from the bottom. For future studies we need high-resolution temperature sensor arrays extending over a range of at least 500 m above the sloping bottom.

Acknowledgments
This research was supported by the TREASURE project (Towards Responsible ExtrAction of Submarine Resources), supported under grant 13273 by the Technology Foundation STW of the Netherlands Organization for Scientific Research (NWO). R/V *Pelagia* cruise 64PE412 was funded by the Topsector Water programme. We thank the captain and the crew of the R/V *Pelagia* for their kind assistance during the sea operations. We thank M. Laan for his enthusiastic development of NIOZ temperature sensors. The construction of these sensors has been financed in part by NWO. Data requests can be directed to hans.van.haren@nioz.nl.

References

Aucan, J., M. A. Merrifield, D. S. Luther, and P. Flament (2006), Tidal mixing events on the deep flanks of Kaena Ridge, Hawaii, *J. Phys. Oceanogr.*, *36*, 1202–1219.

Cimatoribus, A. A., and H. van Haren (2015), Temperature statistics above a deep-ocean sloping boundary, *J. Fluid Mech.*, *775*, 415–435.

Boschen, R. E., A. A. Rowden, M. R. Clark, and J. P. A. Gardner (2013), Mining of deep-sea seafloor massive sulfides: A review of the deposits, their benthic communities, impacts from mining, regulatory frameworks and management strategies, *Ocean Coast. Manage.*, *84*, 54–67.

Collins, P. C., et al. (2013), A primer for the environmental impact assessment of mining at seafloor massive sulfide deposits, *Mar. Policy*, *42*, 198–209.

Cyr, F., and H. van Haren (2016), Observations of small-scale secondary instabilities during the shoaling of internal bores on a deep-ocean slope, *J. Phys. Oceanogr.*, *46*, 219–231.

Dale, A. C., and M. E. Inall (2015), Tidal mixing processes amid small-scale deep-ocean topography, *Geophys. Res. Lett.*, *42*, 484–491, doi:10.1002/2014GL062755.

Desbruyères, D., A. Almeida, M. Biscoito, T. Comtet, A. Khripounoff, N. Le Bris, P. M. Sarradin, and M. Segonzac (2000), A review of the distribution of hydrothermal vent communities along the northern Mid-Atlantic Ridge: Dispersal vs. environmental controls, *Hydrobiologia*, *440*, 201–216.

Dillon, T. M. (1982), Vertical overturns: A comparison of Thorpe and Ozmidov length scales, *J. Geophys. Res.*, *87*, 9601–9613, doi:10.1029/JC087iC12p09601.

Eriksen, C. C. (1982), Observations of internal wave reflection off sloping bottoms, *J. Geophys. Res.*, *87*, 525–538, doi:10.1029/JC087iC01p00525.

German, C., G. P. Klinkhammer, and M. Rudnicki (1996), The Rainbow hydrothermal plume, 36°15′N, MAR, *Geophys. Res. Lett.*, *23*, 2979–2982, doi:10.1029/96GL02883.

Gregg, M. C. (1989), Scaling turbulent dissipation in the thermocline, *J. Geophys. Res.*, *94*, 9686–9698, doi:10.1029/JC094iC07p09686.

Inall, M. E., T. Rippeth, C. Griffiths, and P. Wiles (2005), Evolution and distribution of TKE production and dissipation within stratified flow over topography, *Geophys. Res. Lett.*, *32*, L08607, doi:10.1029/2004GL022289.

Intergovernmental Oceanographic Commission (IOC), Scientific Committee on Oceanic Research (SCOR), and International Association for the Physical Sciences of the Oceans (IAPSO) (2010), *The International Thermodynamic Equation of Seawater—2010: Calculation and Use of Thermodynamic Properties*, Intergovernmental Oceanographic Commission, 196 pp., Manuals and guides no. 56 , UNESCO, Paris.

Khripounoff, A., A. Vangriesheim, P. Crassous, M. Segonzac, A. Colaco, D. Desbruyeres, and R. Barthelemy (2001), Particle flux in the Rainbow hydrothermal vent field (Mid-Atlantic Ridge): Dynamics, mineral and biological composition, *J. Mar. Res.*, *59*, 633–656.

Klymak, J., R. Pinkel, and L. Rainville (2008), Direct breaking of the internal tide near topography: Kaena Ridge, Hawaii, *J. Phys. Oceanogr.*, *38*, 380–399.

Legg, S., and J. Klymak (2008), Internal hydraulic jumps and overturning generated by tidal flow over a tall steep ridge, *J. Phys. Oceanogr.*, *38*, 1949–1964.

Mater, B. D., S. K. Venayagamoorthy, L. S. Laurent, and J. N. Moum (2015), Biases in Thorpe scale estimates of turbulence dissipation. Part I: Assessments from large-scale overturns in oceanographic data, *J. Phys. Oceanogr.*, *45*, 2497–2521.

Oakey, N. S. (1982), Determination of the rate of dissipation of turbulent energy from simultaneous temperature and velocity shear microstructure measurements, *J. Phys. Oceanogr.*, *12*, 256–271.

Sander, S. G., and A. Koschinsky (2011), Metal flux from hydrothermal vents increased by organic complexation, *Nat. Geosci.*, *4*, 145–150.

Sander, S. G., and A. Koschinsky (2016), Trace metal biogeochemistry and ecology of deep-sea hydrothermal vent systems, in *The Export of Iron and Other Trace Metals From Hydrothermal Vents and the Impact on Their Marine Biogeochemical Cycle*, *The handbook of Environ. Chem.*, vol. 50, edited by L. D. Liudmila and V. G. Sergey, pp. 9–24, Springer International Publishing, Switzerland.

Slinn, D. N., and J. J. Riley (1996), Turbulent mixing in the oceanic boundary layer caused by internal wave reflection from sloping terrain, *Dyn. Atmos. Oceans*, *24*, 51–62.

Thorpe, S. A. (1977), Turbulence and mixing in a Scottish loch, *Phil. Trans. R. Soc. London A*, *286*, 125–181.

Thorpe, S. A. (1987), Transitional phenomena and the development of turbulence in stratified fluids: A review, *J. Geophys. Res.*, *92*, 5231–5248, doi:10.1029/JC092iC05p05231.

Thurnherr, A. M., and K. J. Richards (2001), Hydrography and high temperature heat flux of the Rainbow hydrothermal site (36°14′N, Mid-Atlantic Ridge), *J. Geophys. Res.*, *106*, 9411–9426, doi:10.1029/2000JC900164.

van Haren, H. (2017), Exploring the vertical extent of breaking internal wave turbulence above deep-sea topography, *Dyn. Atmos. Oceans*, *77*, 89–99.

van Haren, H., and L. Gostiaux (2012), Detailed internal wave mixing observed above a deep-ocean slope, *J. Mar. Res.*, *70*, 173–197.

van Haren, H., N. Oakey, and C. Garrett (1994), Measurements of internal wave band eddy fluxes above a sloping bottom, *J. Mar. Res.*, *52*, 909–946.

van Haren, H., M. Laan, D.-J. Buijsman, L. Gostiaux, M. G. Smit, and E. Keijzer (2009), NIOZ3: Independent temperature sensors sampling yearlong data at a rate of 1 Hz, *IEEE J. Ocean. Eng.*, *34*, 315–322.

van Haren, H., A. A. Cimatoribus, and L. Gostiaux (2015), Where large deep-ocean waves break, *Geophys. Res. Lett.*, *42*, 2351–2357, doi:10.1002/2015GL063329.

Winters, K. B. (2015), Tidally driven mixing and dissipation in the boundary layer above steep submarine topography, *Geophys. Res. Lett.*, *42*, 7123–7130, doi:10.1002/2015GL064676.